Solar Energy Materials & Solar Cells 294 (2026) 113899

Contents lists available at ScienceDirect

Solar Energy Materials and Solar Cells

journal homepage: www.elsevier.com/locate/solmat

Early degradation of silicon heterojunction PV modules installed on horizontal single-axis trackers in desert climate

A.A. Abdallah [a,*], M. Kivambe [a], M. Abdelrahim [a], M. Elgaili [a], A. Ahmed [a], K. Mroue [a], O. Stroyuk [b], O. Mashkov [b], I.M. Peters [b], C. Buerhop-Lutz [b]

[a] Qatar Environment and Energy Research Institute (QEERI), Hamad bin Khalifa University (HBKU), Qatar Foundation, P.O. Box 34110, Doha, Qatar
[b] Forschungszentrum Juelich GmbH, Helmholtz Institute Erlangen-Nuernberg for Renewable Energy (HI ERN), 91058, Erlangen, Germany

ARTICLE INFO

Keywords:
Horizontal single axis tracker HSAT
Early degradation
Encapsulant
UV fluorescence
NIRA
Bill-of-materials

ABSTRACT

We present our latest findings on the early degradation of photovoltaic (PV) silicon heterojunction (HJT) modules installed in harsh desert climates for about two and half years. The results are compared with the benchmark modules with monofacial and bifacial passivated emitter rear contact (PERC) and passivated emitter rear totally diffused (PERT) technologies installed on a horizontal single-axis tracker (HSAT). These findings showed an early degradation of 62 % of the inspected PV modules induced by their field exposure to a desert climate. Ultraviolet fluorescence (UVF) imaging showed signatures of early degradation of encapsulant materials, while near-infrared absorption spectroscopy (NIRA) identified PV module materials in the field. We found evidence of the use of different encapsulant materials and different variants of the same encapsulant materials by the module manufacturer. In contrast to the PERC PV modules with thermoplastic polyolefin (TPO) and polyolefin elastomer (POE) encapsulants, HJT modules with TPO encapsulants showed distinct UVF patterns indicating early degradation. Similarly, all the HJT PV modules with POE and ethylene vinyl acetate (EVA) encapsulant showed UVF degradation patterns. The PERC-2 PV modules exhibited UVF degradation patterns as well but with no significant change in the maximum power P_{max}. While the P_{max} of the HJT-1, HJT-2a, and HJT-2b dropped by −5.9 %, −3.0 %, and −7.3 %, respectively. The study showed that harsh desert climate induces early encapsulant aging, particularly, glass-glass modules showing the importance of encapsulant material selection.

1. Introduction

The international technology roadmap for photovoltaics (ITRPV) has been shown in the latest edition [1] an increase in the market share of silicon heterojunction (HJT) and back-contact silicon technologies, while tunnel oxide passivated contact (TOPCon) solar cells are still well-appreciated for their cost-effectiveness, compatibility with the manufacturing of PERC technology, and effective carrier transport properties due to their excellent passivation [2–4]. The HJT solar cell is known for its lower temperature coefficient, making it suitable for desert climates with typical high module operating temperatures.

During the last few years, PV module manufacturers have focused on the production of different types of PV modules with various solar cell architectures (PERC, PERT, TOPCon, and HJT), different configurations, such as half-cell, one-third-cells, glass/backsheet, and glass/glass, different wafer sizes (M10, M12), and different module bill of materials (BOM), this versatility resulting in early reliability issues during field operation. Recently, Sen et al. [5,6] have shown different failure modes at the interconnection of busbars and ribbon wires causing power loss of TOPCon and HJT modules that are not observed in PERC modules. For instance, human fingerprints can cause power loss in HJT modules up to 40 % after 4000 h of damp heat (DH) testing.

Using ethylene vinyl acetate (EVA) copolymer encapsulant in TOPCon and HJT PV modules has shown power loss due to degradation in highly humid environments [7]. The corrosion is assumed to result from electrochemical reactions between moisture and acetic acid because of EVA degradation and/or from other contaminants stemming from solder flux and glass, that increase the series resistance (R_s) and cause power loss. For glass/backsheet HJT one-cell mini-modules, a higher degradation rate of 1.5 times the maximum power was reported when using

This article is part of a special issue entitled: SiliconPV 2025 published in Solar Energy Materials and Solar Cells.

* Corresponding author.
E-mail address: aabdallah@hbku.edu.qa (A.A. Abdallah).

https://doi.org/10.1016/j.solmat.2025.113899
Received 29 April 2025; Received in revised form 30 June 2025; Accepted 7 August 2025
Available online 11 August 2025

Fig. 1. Photographs of the front (top) and rear (bottom) of the Horizontal Single Axis (HSAT) testbed installed at the outdoor test facility (Doha, Qatar). Trackers 2, 4, and 6, each consisting of eight strings, will be the focus of this study.

Table 1
Electrical parameters for the commercial PV modules with different cell technologies installed on trackers 2, 4, and 6 of the HSAT testbed. (G/G: glass/glass). Each string consists of 6 PV modules with a total of eight strings.

ID	PV Module Technology	Module Power [W]	String Power [W]	V_{oc} [V]	I_{sc} [A]
PERC-1	Monofacial, G/backsheet, framed	375	2500	41.10	11.60
PERC-2	Bifacial, G/G, framed	375	2500	48.30	9.87
PERC-3a	Bifacial, G/G, half-cell, framed	405	2430	47.40	10.98
PERC-3b	Bifacial, G/G, half-cell, framed	370	2220	47.40	9.83
PERT	Bifacial, G/G, half-cell, frameless	375	2250	47.90	10.12
HJT-1	Bifacial, G/G, half-cell, framed	450	2700	53.14	11.93
HJT-2a	Bifacial, G/G, full-cell, frameless	395	2370	52.94	9.41
HJT-2b	Bifacial, G/G, full-cell, framed	395	2370	53.03	9.26

EVA as compared with polyolefin elastomer (POE) encapsulants [8].

The recent innovations in PV module materials to reduce the cost and improve reliability showed an increased share of application of POE and thermoplastic elastomer (TPO) encapsulants in glass/glass configuration, both yielding improved performance and reduced degradation in terms of resistance to acid-induced corrosion as compared with the EVA encapsulant [9]. However, only a limited number of studies have so far demonstrated increased module durability with these alternative BOMs [10]. The results of accelerated aging tests comparing TPO, POE, and EVA samples are rather scattered, with some studies reporting TPO and POE samples performing better than EVA and others and *vice versa*.

In high operating temperatures and high relative humidity conditions, results from the field tests have shown various TOPCon cell and module materials reliability issues compared with PERC. In the case of HJT contamination, moisture ingress and delamination of the front silver aluminum paste were observed at elevated temperatures and relative humidity. Wu et al. [11] have shown that laser-enhanced contact firing improved contact properties. Moisture-induced contact degradation was reported [7], with the n-type TOPCon cells found much more susceptible to degradation as compared to p-type PERC cells. The latter study also pointed out that new encapsulant materials such as POE and TPO showed improved protection of the metal grid. The investigation by Sen et al. [12] showed an increase in the series resistance of the front contact of TOPCon, both sides of the HJT cell, and the rear side of the PERC cell due to metal contact corrosion. HJT modules can experience moisture-induced degradation when encapsulated with the frontal EVA layer [8,13,14].

In this situation, early detection of PV module degradation is crucial for predictive maintenance and the long-term performance of PV systems. Among other more conventional techniques, UV fluorescence (UVF) imaging has recently been proven to be a reliable, fast, and direct method for detecting polymer (encapsulant and/or backsheet) degradation [15,16]. At that, the fluorescence emitted by the PV module polymer components when exposed to UV light can be used as a general indication of polymer material aging.

Overall, further extensive research is essential to tackle the challenges of high UV irradiance and high operating temperature-induced degradation in TOPCon and HJT technologies, particularly in hot climates, such as the desert climate of Qatar. Detailed knowledge about the severity of these new failure modes for the Qatar climate is of key importance, comparable to many sun-rich, PV-friendly regions around the globe and close to the equator. Considering this, the main objective of this study is to investigate the reliability of new PV technologies, e.g., HJT bifacial, glass/glass PV technologies that showed signs of aging after 2 years of field exposure in desert climates and compare it with benchmark PERC technologies.

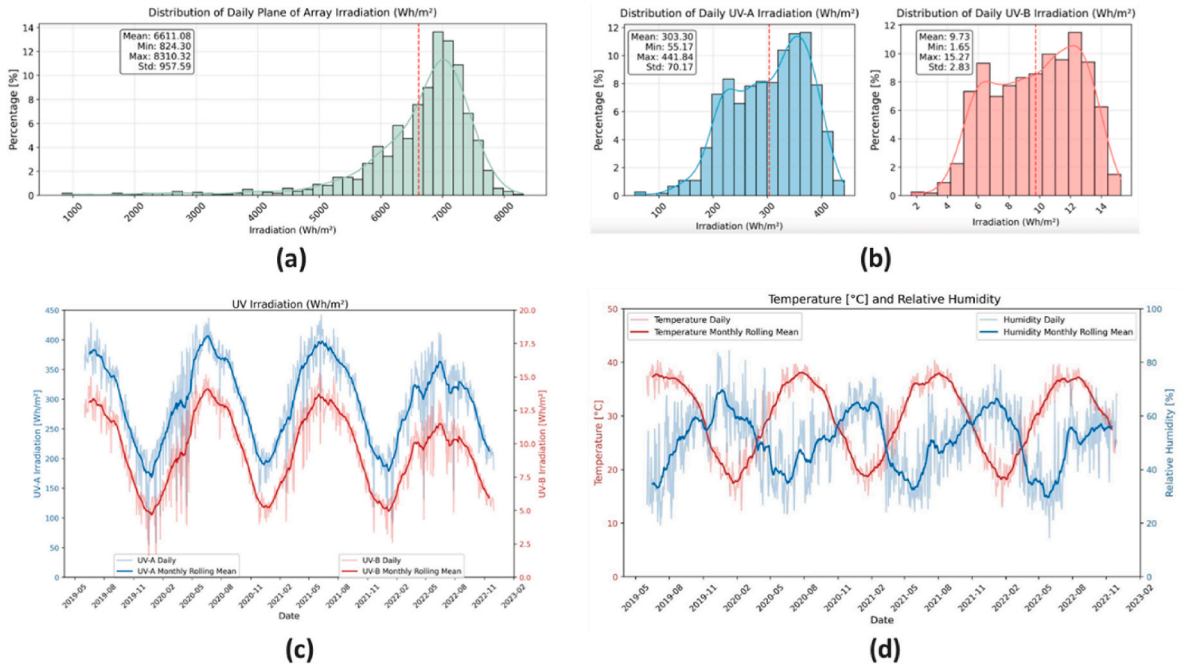

Fig. 2. (a) Daily distribution of the plane of array POA irradiation, (b) daily distribution of the UV-A and UV-B, (c) monthly distribution of the UV-A and UV-B, and (d) seasonal variation of the ambient temperature and relative humidity measured at the outdoor test facility (Doha, Qatar).

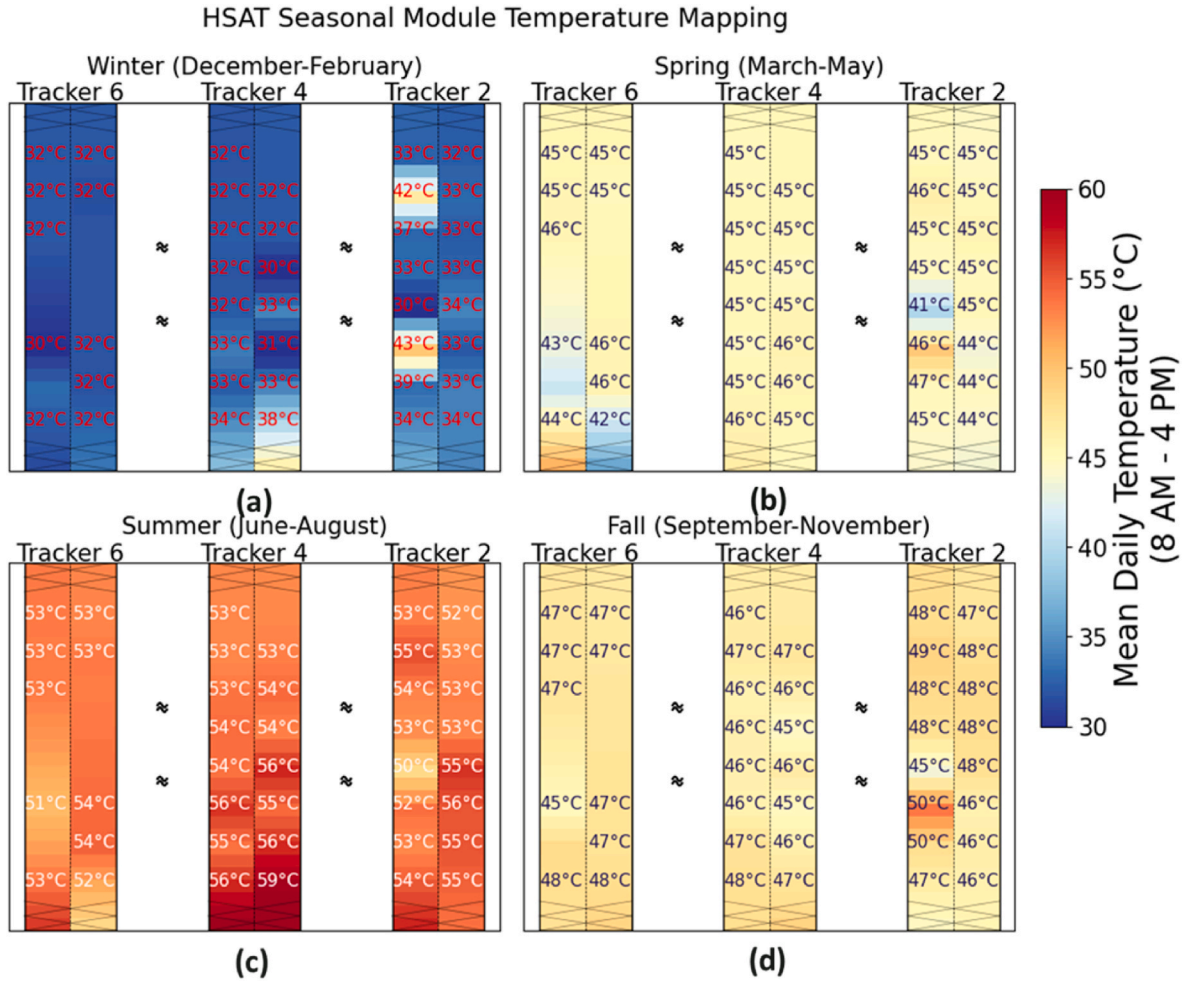

Fig. 3. Module temperature measured on trackers 2, 4, and 6. High PV modules measured during the summer months compared with the winter months.

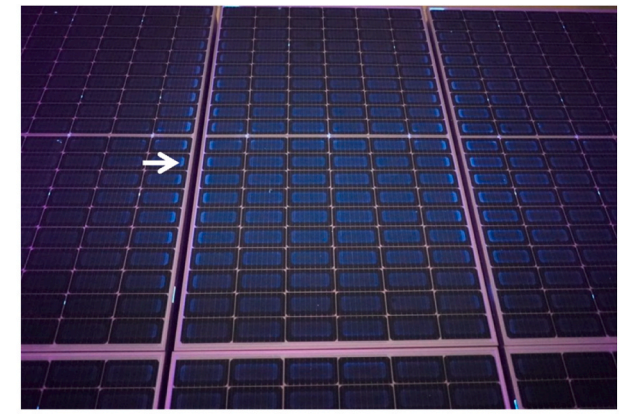

(a)

(b)

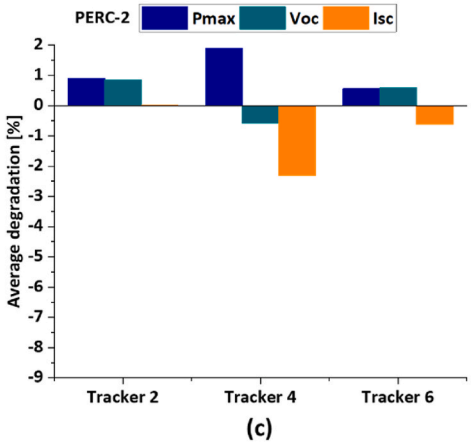

(c)

Fig. 4. Early degradation in bifacial PERC-2 PV modules with framed glass/glass configuration installed on trackers 2, 4, and 6: (a) UVF degradation pattern of the front side indicated by an arrow, (b) UVF pattern on the rear side indicated by an arrow, and (c) variations in the average measured electrical parameters P_{max}, I_{sc}, and V_{oc}.

2. Methodology

2.1. Outdoor test facility

Generally, most of the utility-scale PV projects in the Middle East use horizontal single-axis tracking (HSAT) with bifacial technology to improve the energy yield, resulting in a low leveraged cost of electricity (LCOE) in different locations [17]. The present study has been performed on an HSAT testbed installed at the Outdoor Test Facility (OTF) in Doha (latitude 25.33°N, longitude 51.43°E). The HSAT system was installed in April 2022 to study performance and reliability in desert climates using different PV technologies, row-to-row distance, ground coverage ratio, and the edge effect on solar irradiation received on the rear side of the modules.

In this paper, we focus on field inspection and PV module materials aging during the early testing period from April 2022 to December 2024. The weathering data including module temperature and humidity were collected with a 1-min resolution. Fig. 1 shows a photograph of the front and rear sides of the HSAT testbed installed at the OTF. The trackers under study are tracker numbers 2, 4, and 6, with two dummy modules installed at the edge of each row for irradiance, wind, and temperature uniformity purposes.

2.2. PV system

The present study focuses on trackers 2, 4, and 6, with a total of 144 PV modules with PERC, PERT, and HJT cell technologies. Table 1 shows the rated power, string power, open circuit voltage $V_{oc,}$ and short circuit current I_{sc} obtained from the manufacturer data sheet for the tested modules. The PV system performance and meteorological data were monitored during the testing period from April 2022 to December 2024.

2.3. PV system inspection

The PV modules returned from the field for the lab tests were first inspected visually to detect any visual irregularities. The electrical parameters were performed at the Standard Testing Conditions (STC) and compared with the initial measurement (at time zero). Note, the initial measurements were performed after stabilization according to the standards. Next, indoor Electroluminescence (EL) imaging was performed in a dark room to investigate degradation features in PV modules, e.g., the presence of cell cracks, electrical defects in cells, and interconnections. Images were taken at a biased current equal to the module I_{sc} and compared with the initial EL images, collected before installation in the field.

Ultraviolet Fluorescence (UVF) imaging detects encapsulant degradation by exciting fluorophores with UV light (typically 340–365 nm). When an encapsulant degrades, it emits visible light (450–550 nm) upon UV excitation. The fluorescence intensity correlates directly with degradation severity. To provide a comprehensive assessment of PV system reliability, non-destructive UVF imaging, performed with a portable UVF-Spot illumination system (Bright Spot Automation) with a Sony A7SIII camera for image acquisition. The UVF camera was used to detect PV modules' aging in the dark directly at the OTF. The camera was equipped with a long-pass filter cutting incoming light below 400 nm.

Finally, Near-infrared absorption (NIRA) spectroscopy was performed at the OTF using NIRONe sensor S2.2 (Spectral Engines, Finland) with a spectral range of 1750–2150 nm and a spectral resolution of ca. 10 nm for non-destructive polymer BOM identification and aging analysis.

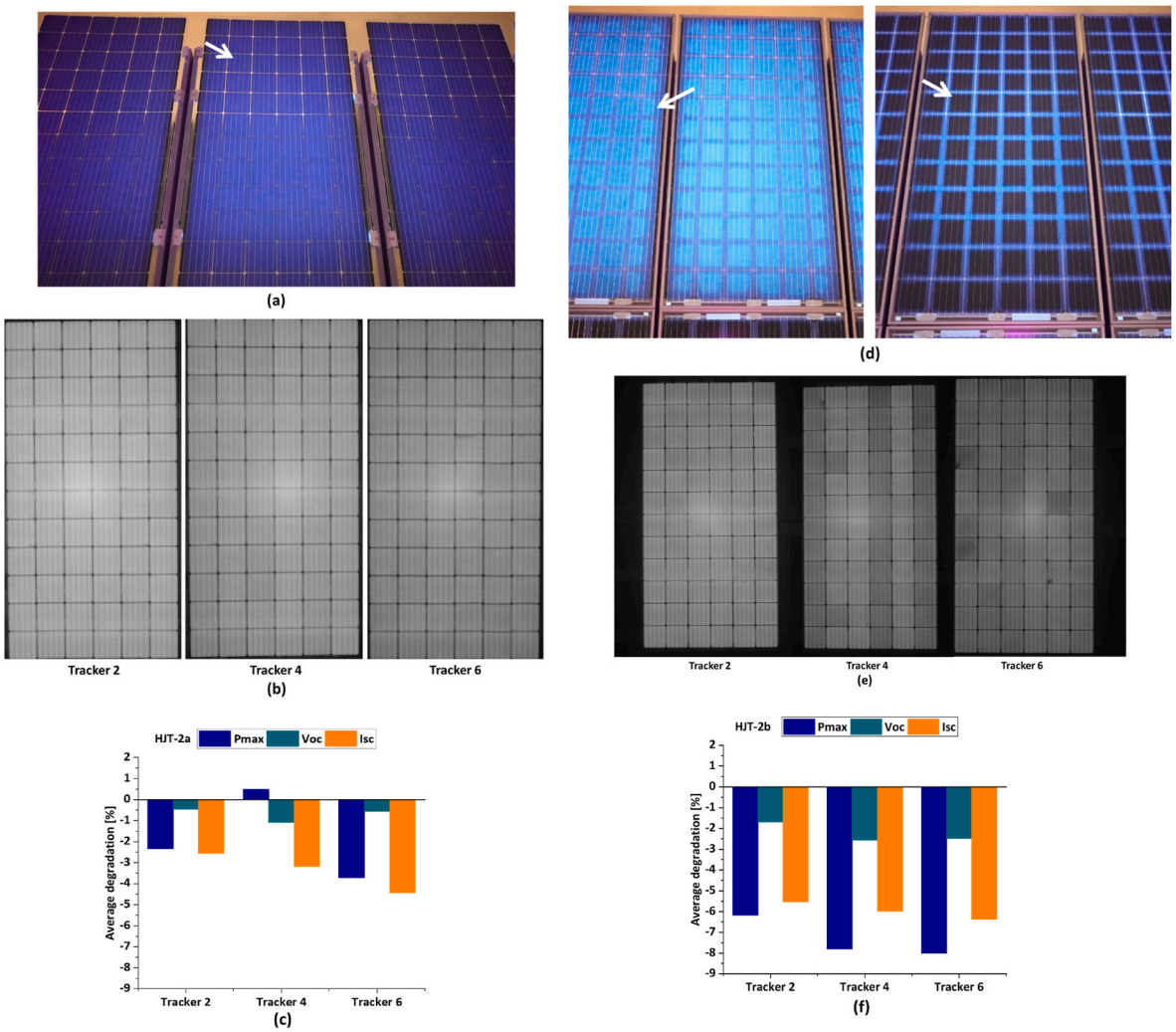

Fig. 5. Characteristics of frameless bifacial glass/glass PV modules with the HJT-2a (a–c) and HJT-2b (d–f) cell technologies installed on trackers 2, 4, and 6: (a, d) UVF degradation patterns indicated by an arrow, (b, e) EL images of the modules from tracker 2, 4, and 6, (c, f) Indoor STC-measured electrical parameters P_{max}, I_{sc} and V_{oc} values normalized to the datasheet.

3. Results

3.1. Meteorological data

The discussion of the early degradation of PV modules detected in the present study requires a characterization of the climatic conditions at the PV site. The typical desert climate at the OTF is characterized by high solar irradiation with a high UV irradiation fraction, high average ambient temperature, and high average albedo. A mean daily plane of array (POA) irradiation of 6.6 kWh/m^2/day was measured (Fig. 2a), while the mean daily distribution of the UV-A and UV-B irradiation was 303 and 10 Wh/m^2, respectively (Fig. 2b). Note the average irradiation time in Doha within one year is about 4461 h. Fig. 2c shows the monthly distribution of UV-A and UV-B during the testing period, with an increase during the summer months.

The maximum ambient temperature and relative humidity values during the summer and winter seasons are shown in Fig. 2c, with a daily ambient temperature and relative humidity reaching 40 °C and 70 %, respectively. A high average albedo of 40 % originating from a strong reflected irradiance from the ground (gravel) at the OTF has been reported in our previous study [18].

Fig. 3 shows the PV module temperature measured on the rear side of the PV module at the center of the string on trackers 2, 4, and 6. On average, PV modules can reach 58 °C during the summer months (June–August) and 35 °C during the winter months (December–February). These variations are augmented by the difference in solar irradiance received on the PV modules throughout the year, ranging from 5.3 to 8.8 kWh/m^2/day. Further, the rear side irradiance depends on the row-to-row shading and the ground coverage ratio (GCR). For the bifacial PV module, the energy yield also depends on solar irradiation, while the PV module materials' longevity will depend, among other factors, on the fraction of UV irradiation and the module temperature. At that, the high UV-A and UV-B components and high module temperatures are expected to accelerate the PV module encapsulants.

3.2. PV module material degradation

The early aging of PV modules on trackers 2, 4, and 6 was detected by UVF imaging. Fig. 4a and b shows exemplary UVF degradation patterns observed at the front and rear sides of the framed glass/glass bifacial PERC technology. The UVF patterns at the front differ from those at the rear. The fluorescence intensity at the rear increases gradually towards the module edge. The appearance of gradients in the UVF patterns at the module edges (increase in fluorescence intensity toward the edge) most probably indicates the path of water and oxygen ingress. At that, the indoor EL images of these PV modules (not shown here) do not show any sign of degradation.

The bar plot in Fig. 4c shows the results of the indoor STC-measured

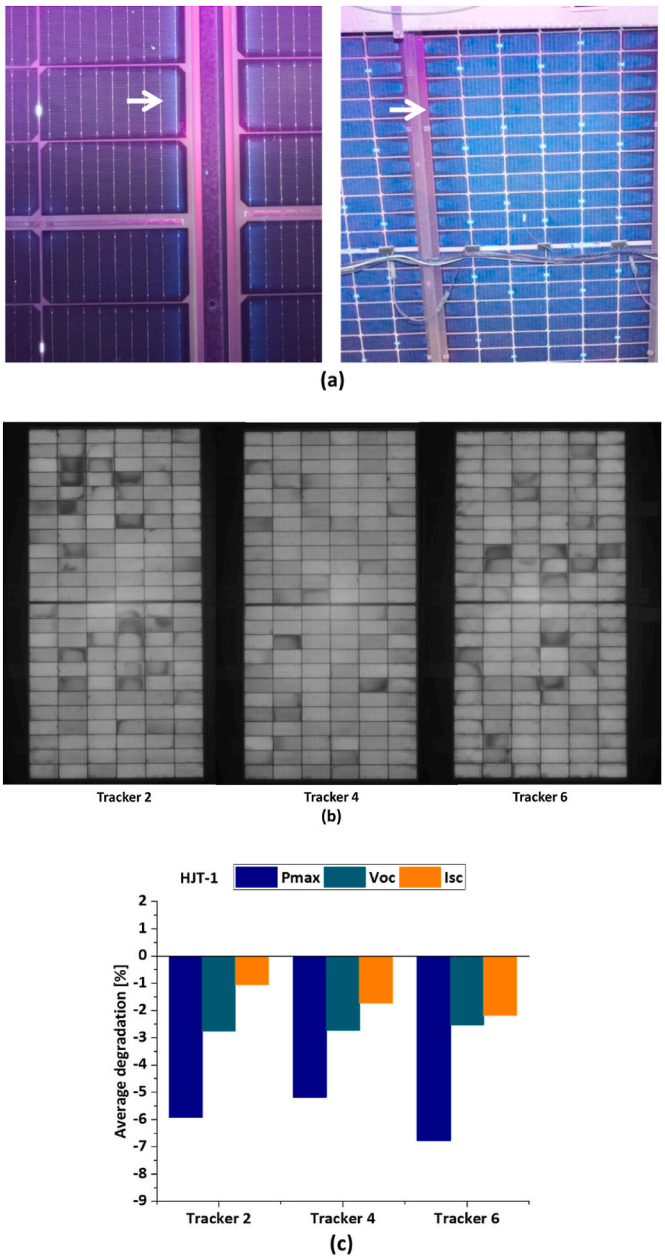

Fig. 6. Characteristics of bifacial framed glass/glass PV modules with the HJT-1 cell technology installed on trackers 2, 4, and 6: (a) UVF degradation pattern at the front (left) and at the rear (right) indicated by an arrow, (b) EL images of the modules from tracker 2, 4, and 6, (c) the average variation of P_{max}, $I_{sc,}$ and V_{oc} normalized to the datasheet values.

electrical parameters P_{max}, $I_{sc,}$ and V_{oc} normalized to the datasheet values. The average change in the electrical parameters is within the measurement uncertainty of the Sun simulator ±2 %. Therefore, while the first changes of the encapsulant material are visible by UVF, no change in the PV module P_{max} is detected.

Fig. 5 shows the UVF degradation pattern of frame and frameless glass/glass bifacial modules with HJT-2a and HJT-2b cell technologies stemming from the same manufacturer, revealing different geometry of UVF degradation patterns for the frameless modules (Fig. 5a) compared with the framed modules (Fig. 5d). These differences can indicate the use of different encapsulant materials and/or the same encapsulant (POE) but with different additives (see section 3.3 for details on the encapsulant material identification). For the HJT-2b modules with frame, both dark fluorescence area between the solar cells (left) and the darker UVF image under the solar cells (right) were observed (Fig. 5d). This may indicate different adhesion properties of the encapsulant and, therefore, different lamination processes.

For the frameless modules, the P_{max} drops by average −3.0 % (Fig. 5c), while for the framed modules, the drop in the P_{max} by −7.3 % was observed (Fig. 5f). For the HJT-a cell technology, the drop in P_{max} is associated with a drop in the I_{sc} values, while for the HJT-2b technology, the drop in P_{max} is associated with a drop on both I_{sc} and V_{oc}. Degradation of the encapsulant properties is expected to impact the I_{sc}. The EL images of the PV modules (Fig. 5b and e) did not show any sign of cell or module degradation after outdoor exposure.

Fig. 6 shows exemplary UVF patterns of the bifacial framed glass/glass module with HJT-1 cell technology. While the front side (Fig. 6a (left)) shows a weak UVF pattern at the edge, the rear side (Fig. 6ba (right)) shows a strong UVF pattern with a gradual increase of the UVF intensity towards the edge. This non-uniform aging pattern indicates that the encapsulant has degraded more strongly at the module edges potentially due to the ingress of moisture and oxygen from the module edge accelerating the chemical and physical aging of the polymer encapsulant.

The EL images on Fig. 6b show cell mismatch (dark inactive cell areas). Fig. 6c shows a strong power loss, the P_{max} of the module from tracker 2, 4, and 6 drops by average −5.9 %, which is associated with a drop on the V_{oc}. Therefore, we can conclude that both polymer and cell degradation are responsible for the power drop of the HJT-1 on tracker 2, 4 and 6.

Fig. 7a shows the PERT bifacial glass/glass module with encapsulant yellowing at the fixation points most probably caused by a high mechanical stress concentration at these spots. This degradation can be seen as brighter UV fluorescence spots in Fig. 7b. Further, because of edge seal aging shown in Fig. 7c, a shady spot on the UV image was observed, due to the ingress of moisture and oxygen through the degraded edge seal.

3.3. Identification of PV module materials

Polymer components of tested PV modules, in particular, the transparent encapsulant of the front and back sides of the modules, were identified using NIRA spectroscopy using a miniature NIR sensor NIR-One S2.2. The measurements were performed directly on the OTF and analyzed using a library of non-cross-linked reference encapsulant samples provided by an industrial partner. The NIRA inspection identified three types of encapsulants used in the tested modules, including ethylene vinyl acetate (EVA) copolymer, thermoplastic polyolefin (TPO), and polyolefin elastomer (POE). At that, a single sort of EVA, two different sorts of TPO, as well as four different versions of PEO were identified (see Table 2). Fig. 8 presents an exemplary collection of NIRA spectra collected for three different encapsulant types along with the corresponding references.

Fig. 8a shows reference and field spectra of EVA encapsulants revealing characteristic vibrational bands of -C-H in aliphatic polyolefin backbone, O-H in adsorbed water, and carbonyl C=O in the acetate group, the latter unambiguously indicating that both spectra belong to the EVA encapsulant. Minor differences in the shape of the reference (Hanwha HEP-02T, 0.41 mm) and field spectra can be assigned to the effect of cross-linking in the case of the field sample.

Fig. 8b shows exemplary spectra of two types of TPO encapsulant (abbreviated as TPO1 and TPO2) identified based on the general similarity of the spectra to the reference TPO sample (Betterrial TPO, 0.50 mm). While both TPO1 and TPO2 are similar to the reference, they show distinct differences in the fine structure of the spectra in the range of 1900–2050 nm. While the exact assignment of these bands comes beyond the scope of the present work, the differences can tentatively be related to variations in additive composition. The identification of these additives would require destructive sampling of polymers from a sacrificial module, which cannot be done for the present OTF still being

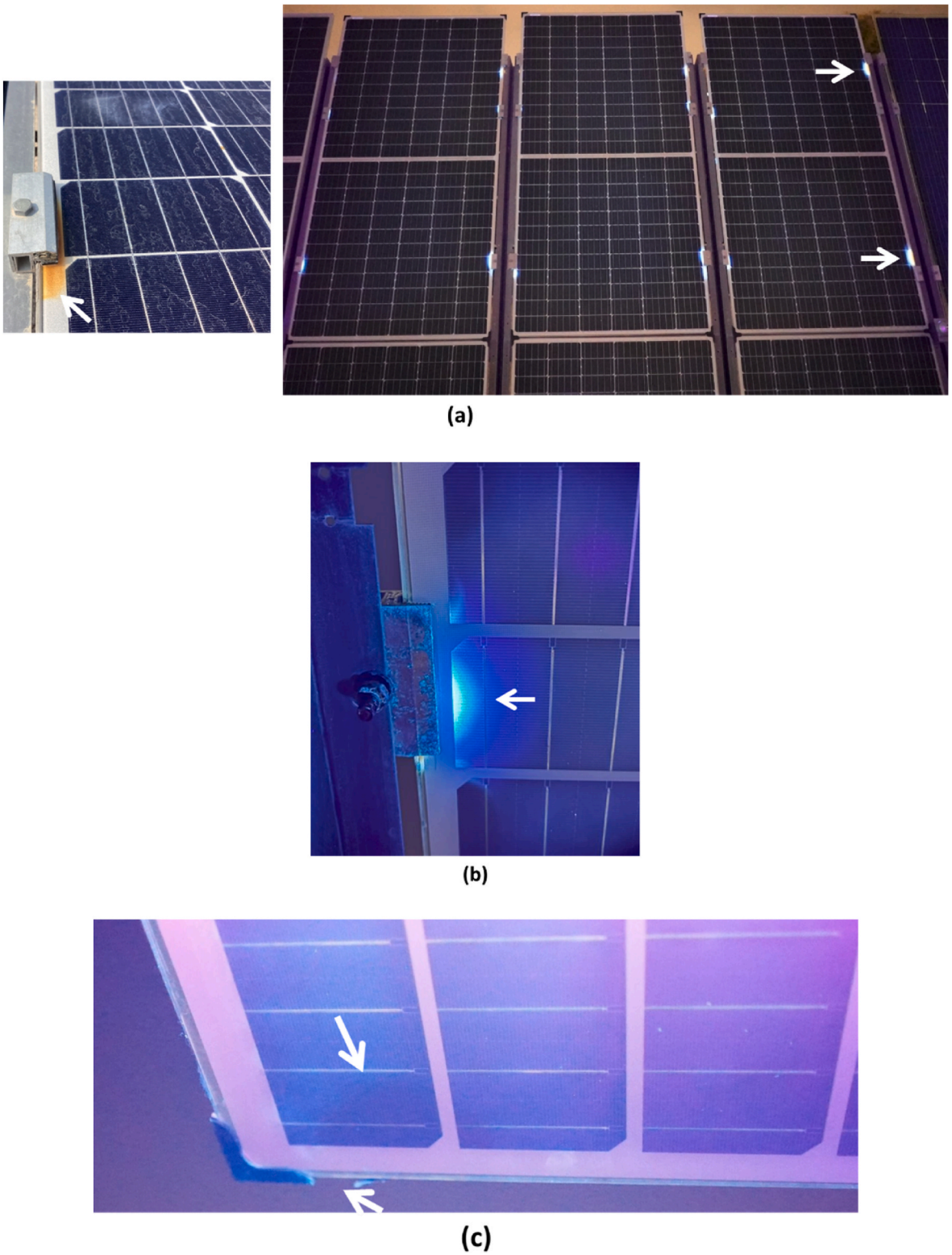

Fig. 7. Characteristics of bifacial frameless glass/glass PV modules with the PERT cell technology installed on trackers 2, 4, and 6: (a) photograph of the encapsulant yellowing at the fixation point indicated by an arrow, (b) UVF pattern showing the degradation of the encapsulant with high-intensity UVF spots at the module fixation point indicated by an arrow, (c) UVF image showing edge seal degradation and dark area indicated by arrows.

during active observation and exploitation.

A similar spectral analysis was applied to identify four different versions of POE encapsulants (POE1, POE2, POE3, and POE4, see Fig. a1c). The spectra of POE polymers show the presence of aliphatic -C-H vibrations but no C=O-related features, allowing POE as well as the above-discussed TPO to be clearly distinguished from the EVA samples. As in the case of TPO, POE samples show general similarity to the POE reference (DPHWC, 0.5 mm) but reveal minor spectral variations in the range of 1900–2100 nm, indicating, most probably, differences in the loading and nature of additives. While fluctuations in C/O and C/H

Table 2
Summary of front and rear encapsulant materials detected by NIRA sensors. Numbers behind the cell technology indicate different manufacturers and numbers behind encapsulant materials indicate differences in additives.

String ID	Encapsulant		Comments
	Front	Rear	
Tracker 2			
PERC-1	TPO	TPO1	No degradation pattern was observed on the UVF pattern
PERC-2	POE1	POE2	Fig. 4, UVF degradation pattern at the front and back.
	POE1	POE1	Different BOM.
PERC-3a	TPO	POE1	No degradation was observed on the UVF pattern
PERC-3b	POE1	POE3	No degradation was observed on the UVF pattern.
	POE1	POE2	Different BOM.
PERT	POE1	POE1	Fig. 7, yellowing at the fixation point, degradation of the edge seal.
HJT-1	EVA	EVA	Fig. 6a, UVF degradation pattern at the front. P_{max} drops by −6.0 %.
HJT-2a	POE4	POE4	Fig. 5a, UVF degradation pattern at the front.
	POE4	POE3	P_{max} drops by −2.2 %
HJT-2b	POE4	POE3	Fig. 5b, UVF degradation pattern at the front. Different BOM. P_{max} drops by −6.1 %
Tracker 4			
PERC-1	TPO	TPO1	No degradation was observed on the UVF pattern.
PERC-2	POE1	POE2	Fig. 4, UVF degradation pattern at the front and back.
PERC-3a	TPO	POE1	No degradation was observed on the UVF pattern.
PERC-3b	POE1	POE2	No degradation was observed on the UVF pattern. Different BOM.
	POE1	POE3	
PERT	POE1	POE1	Fig. 7, yellowing at the fixation point, degradation of the edge seal.
HJT-1	EVA	EVA	Fig. 6a, UVF degradation pattern at the front. P_{max} drops by −5.1 %.
HJT-2a	POE4	POE3	Fig. 5a, UVF degradation pattern at the front. Different BOM. P_{max} drops by −3.0 %.
	POE4	POE4	
HJT-2b	POE4	POE3	Fig. 5b, UVF degradation pattern at the front. P_{max} drops by −7.8 %.
Tracker 6			
PERC-1	TOP	TOP1	No degradation was observed on the UVF pattern.
PERC-2	POE1	POE2	Fig. 4, UVF degradation pattern at the front and back.
PERC-3a	POE1	POE1	No degradation was observed on the UVF pattern.
PERC-3b	EVA	POE1	No degradation was observed on the UVF pattern. Different BOM.
	EVA	EVA	
PERT	POE4	POE1	Fig. 7, yellowing at the fixation point, degradation of the edge seal. Difference BOM.
	POE4	POE3	
HJT-1	POE1	EVA	Fig. 6a, UVF degradation pattern at the front. Different BOM. P_{max} drops by −6.8 %.
	POE1	POE2	
HJT-2a	TPO	POE4	Fig. 5a, UVF degradation pattern at the front. Different BOM. P_{max} drops by −3.8 %
	TPO	POE3	
HJT-2b	POE4	POE3	Fig. 5d, UVF degradation pattern at the front. P_{max} drops by −8.0 %.

ratios were observed (Fig. 8), attribution to specific performance losses is confounded by missing t = 0 data and multi-factor field degradation.

An overview of the front and rear encapsulant materials identified using the NIRA sensors in the field is shown in Table 2. The spectral findings can be summarized together with the observations by UVF imaging as follows:

a) The PV modules with HJT cell technologies revealed a variety of encapsulant types, including POE, EVA, a combination of POE and EVA, and a combination of TPO and POE, all showing degradation patterns in UVF images.
b) TPO encapsulant was used in the module string with PERC-1 technology (trackers 2, 4, and 6) and a combination of TPO with POE - in module string with PERC-3a technology (trackers 2 and 4). These modules showed no UVF degradation pattern, while the TPO encapsulant used in the string with HJT-2a technology (tracker 6) revealed distinct UVF degradation patterns.
c) Different encapsulant materials were used by the manufacturer in the PV modules with the same cell technology, e.g., EVA and POE were used in the module string with PERC -3a and HJT-1 cell technologies (tracker 6).
d) Different versions of the same encapsulant materials were used by the manufacturer (e.g., POE1, POE2, etc.), potentially by using different additives, as exemplified by POE encapsulant in the module strings with PERC-2, PERC-3b, and HJT-2a cell technologies.

Fig. 9 shows the summary of the data collected for all inspected PV modules. From 144 inspected PV modules, 90 modules (62 %) showed the presence of a UVF pattern (indicated in red), indicating the early polymer aging after two and half years of operation in a desert climate. All PV modules with the HJT cell technology and POE encapsulants, as well as bifacial glass/glass PV modules with PERT cell technology and EVA encapsulants, showed these early signs of degradation. At that, the modules with PERT cell technology did not show any degradation in P_{max}, but the UVF inspection revealed encapsulant degradation at the module fixation point.

In summary, different UVF degradation patterns of the encapsulant material were observed after 2 and a half years of operation in desert climates. These different degradation patterns can be explained by:

(1) the ingress of water and oxygen at the module edge for both frame and frameless glass/glass modules (Figs. 4 and 6), especially at the rear gradients, was observed,
(2) the use of different front and rear encapsulant materials (see Table 2) was revealed by UVF and NIRA field tests,
(3) the use of different encapsulant materials and/or different types of the same encapsulant material with different additives, namely TPO, POE, and EVA, cause different UVF degradation patterns (as in Fig. 5),
(4) for frameless modules, the degradation of the edge seal was observed causing water and oxygen ingress inward the module (see Fig. 7),
(5) the presence of a UVF degradation pattern is not necessarily associated with power loss (see Fig. 4).

4. Conclusion

This paper reveals early encapsulant degradation in glass/glass PV modules after 2.5 years in Qatar's desert climate. Field characterization using UVF imaging and NIRA spectroscopy was identified. The results showed that 62 % of modules exhibited UVF patterns, indicating early encapsulant degradation. Here is a summary of the PV module technology-specific trends:

- All HJT bifacial modules (framed/frameless) showed TPO/POE/EVA degradation, with significant P_{max} losses (−5.9 % to −7.3 %).
- PERC bifacial modules with POE encapsulants degraded, while TPO/POE/EVA variants remained stable.
- PERC monofacial (glass/backsheet) showed no degradation or P_{max} losses.
- PERT bifacial modules demonstrated minimal P_{max} loss (−0.7 %), contrasting with HJT's pronounced degradation.

These results underscore UVF's value in quality control for desert-deployed PV systems.

CRediT authorship contribution statement

A.A. Abdallah: Writing – review & editing, Writing – original draft, Methodology, Conceptualization. **M. Kivambe:** Writing – review &

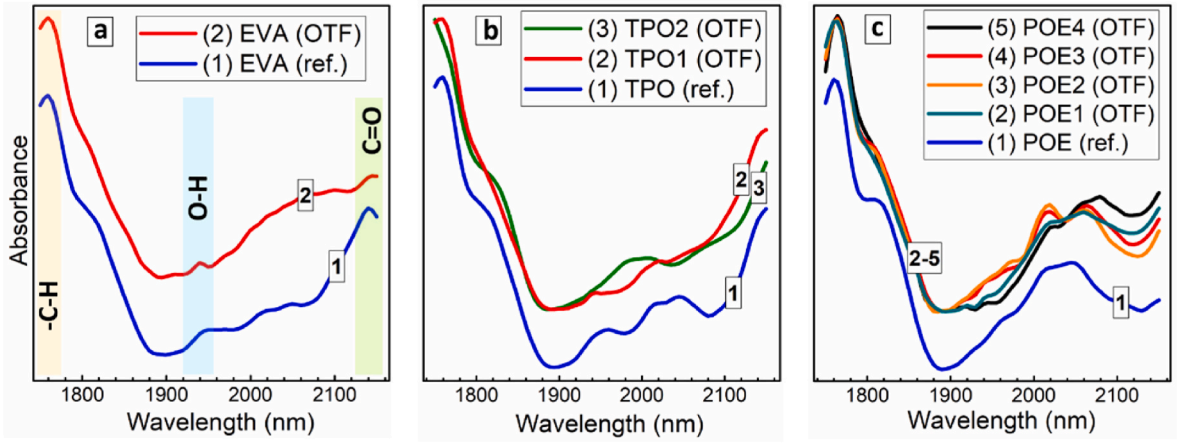

Fig. 8. Exemplary spectra of reference and field-registered (at the OTF) NIRA spectra of EVA, TPO, and POE encapsulants. Reference spectra are artificially shifted along the Y-axis.

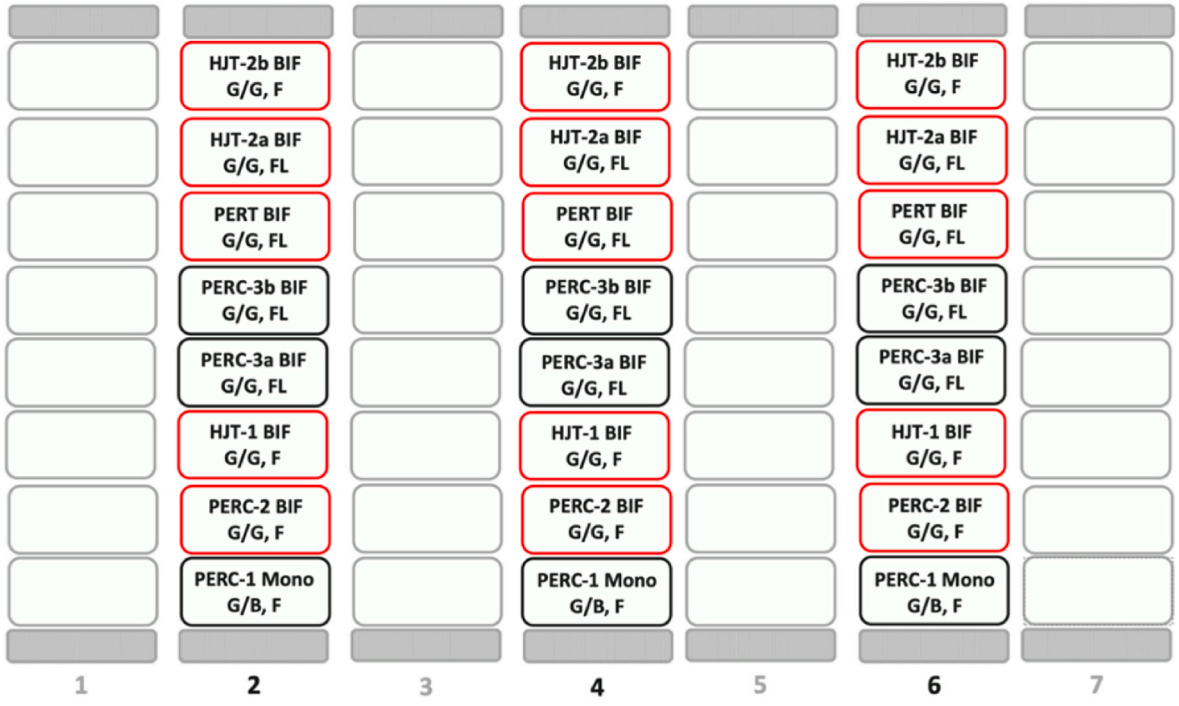

Fig. 9. *Schematic of the HSAT system with different commercial PERC, HJT, and PERT cell technologies.* Only the 144 PV modules installed on trackers 2, 4, and 6 under study are shown. Each string consists of 6 PV modules. *BIF: bifacial, Mono: monofacial, G/G: glass/glass, G/B: glass/backsheet, F: frame, FL: frameless. The PV strings that showed PV module degradation are indicated in red. (For interpretation of the references to colour in this figure legend, the reader is referred to the Web version of this article.)*

editing. **M. Abdelrahim:** Formal analysis. **M. Elgaili:** Formal analysis. **A. Ahmed:** Formal analysis. **K. Mroue:** Writing – review & editing, Methodology. **O. Stroyuk:** Writing – review & editing, Methodology, Formal analysis. **O. Mashkov:** Writing – review & editing, Methodology, Formal analysis. **I.M. Peters:** Writing – review & editing, Resources. **C. Buerhop-Lutz:** Writing – review & editing, Writing – original draft, Methodology, Formal analysis, Conceptualization.

Declaration of competing interest

The authors declare that they have no known competing financial interests or personal relationships that could have appeared to influence the work reported in this paper.

Acknowledgment

This publication was made possible by NPRP Grant # NPRP11S-1220-170110 from the Qatar National Research Fund (a member of Qatar Foundation), the findings herein reflect the work and are solely the responsibility, of the authors. HI ERN thanks for the support by the German Federal Ministry for Economic Affairs and Climate Action (projects dig4morE," FKZ: 03EE1090B, "Rembup" FKZ: 03WR021F), the Helmholtz Association in the framework of the innovation platform "Solar TAP" (No. 714-62150-3/1 (2023)) and Zentrales Innovation-sprogramm Mittelstand (ZIM, project "RobInspec" No. 16KN083044).

Data availability

Data will be made available on request.

References

[1] International Technology Roadmap for Photovoltaics ITRPV fifteenth ed., (n.d.).
[2] F. Feldmann, M. Bivour, C. Reichel, M. Hermle, S.W. Glunz, Passivated rear contacts for high-efficiency n-type Si solar cells providing high interface passivation quality and excellent transport characteristics, Sol. Energy Mater. Sol. Cells 120 (2014) 270–274, https://doi.org/10.1016/j.solmat.2013.09.017.
[3] A. Richter, R. Müller, J. Benick, F. Feldmann, B. Steinhauser, C. Reichel, A. Fell, M. Bivour, M. Hermle, S.W. Glunz, Design rules for high-efficiency both-sides-contacted silicon solar cells with balanced charge carrier transport and recombination losses, Nat. Energy 6 (2021) 429–438, https://doi.org/10.1038/s41560-021-00805-w.
[4] B. Liao, X. Wu, W. Wu, C. Liu, S. Ma, S. Wang, T. Xie, Q. Wang, Z. Du, W. Shen, X. Li, W. Li, B. Hoex, Tube-type plasma-enhanced atomic layer deposition of aluminum oxide: enabling record lab performance for the industry with demonstrated cell efficiencies >24, Prog. Photovoltaics Res. Appl. 31 (2023) 52–61, https://doi.org/10.1002/pip.3607.
[5] C. Sen, H. Wang, M.U. Khan, J. Fu, X. Wu, X. Wang, B. Hoex, Buyer aware: three new failure modes in TOPCon modules absent from PERC technology, Sol. Energy Mater. Sol. Cells 272 (2024) 112877, https://doi.org/10.1016/j.solmat.2024.112877.
[6] C. Sen, H. Wang, X. Wu, M.U. Khan, C. Chan, M. Abbott, B. Hoex, Four failure modes in silicon heterojunction glass-back sheet modules, Sol. Energy Mater. Sol. Cells 257 (2023) 112358, https://doi.org/10.1016/j.solmat.2023.112358.
[7] P.M. Sommeling, J. Liu, J.M. Kroon, Corrosion effects in bifacial crystalline silicon PV modules; interactions between metallization and encapsulation, Sol. Energy Mater. Sol. Cells 256 (2023) 112321, https://doi.org/10.1016/j.solmat.2023.112321.
[8] J. Karas, A. Sinha, V.S.P. Buddha, F. Li, F. Moghadam, G. TamizhMani, S. Bowden, A. Augusto, Damp heat-induced degradation of silicon heterojunction solar cells with Cu-plated contacts, IEEE J. Photovoltaics 10 (2020) 153–158, https://doi.org/10.1109/JPHOTOV.2019.2941693.
[9] IEA PVPS Task 13 Report, (n.d.).
[10] G. Oreski, A. Omazic, G.C. Eder, Y. Voronko, L. Neumaier, W. Mühleisen, C. Hirschl, G. Ujvari, R. Ebner, M. Edler, Properties and degradation behaviour of polyolefin encapsulants for photovoltaic modules, Prog. Photovoltaics Res. Appl. 28 (2020) 1277–1288, https://doi.org/10.1002/pip.3323.
[11] X. Wu, X. Wang, W. Yang, J. Nie, J. Yuan, M.U. Khan, A. Ciesla, C. Sen, Z. Qiao, B. Hoex, Enhancing the reliability of TOPCon technology by laser-enhanced contact firing, Sol. Energy Mater. Sol. Cells 271 (2024) 112846, https://doi.org/10.1016/j.solmat.2024.112846.
[12] C. Sen, X. Wu, H. Wang, M.U. Khan, L. Mao, F. Jiang, T. Xu, G. Zhang, C. Chan, B. Hoex, Accelerated damp-heat testing at the cell-level of bifacial silicon HJT, PERC and TOPCon solar cells using sodium chloride, Sol. Energy Mater. Sol. Cells 262 (2023) 112554, https://doi.org/10.1016/j.solmat.2023.112554.
[13] D. Adachi, T. Terashita, T. Uto, J.L. Hernández, K. Yamamoto, Effects of SiOx barrier layer prepared by plasma-enhanced chemical vapor deposition on improvement of long-term reliability and production cost for Cu-plated amorphous Si/crystalline Si heterojunction solar cells, Sol. Energy Mater. Sol. Cells 163 (2017) 204–209, https://doi.org/10.1016/j.solmat.2016.12.029.
[14] H. Park, J. Jeong, E. Shin, S. Kim, J. Yi, A reliability study of silicon heterojunction photovoltaic modules exposed to damp heat testing, Microelectron. Eng. 216 (2019) 111081, https://doi.org/10.1016/j.mee.2019.111081.
[15] S. Kumar, H. Alhamadani, S. Hassan, A. Alheloo, H. Hanifi, J. Joseph John, G. Mathiak, V. Alberts, Comparative investigation and analysis of encapsulant degradation and glass abrasion in desert exposed photovoltaic modules, in: 2021 IEEE 48th Photovolt. Spec. Conf. PVSC, IEEE, Fort Lauderdale, FL, USA, 2021, pp. 793–798, https://doi.org/10.1109/PVSC43889.2021.9519122.
[16] D.B. Sulas-Kern, S. Johnston, M. Owen-Bellini, K. Terwilliger, J. Meydbray, L. Spinella, A. Sinha, L.T. Schelhas, D.C. Jordan, UV-fluorescence imaging of silicon PV modules after outdoor aging and accelerated stress testing, in: 2020 47th IEEE Photovolt. Spec. Conf. PVSC, IEEE, Calgary, AB, Canada, 2020, pp. 1444–1448, https://doi.org/10.1109/PVSC45281.2020.9300901.
[17] C.D. Rodríguez-Gallegos, H. Liu, O. Gandhi, J.P. Singh, V. Krishnamurthy, A. Kumar, J.S. Stein, S. Wang, L. Li, T. Reindl, I.M. Peters, Global techno-economic performance of bifacial and tracking photovoltaic systems, Joule 4 (2020) 1514–1541, https://doi.org/10.1016/j.joule.2020.05.005.
[18] S. Dittmann, L. Burnham, B. Figgis, R. Gottschalg, K.-S. Kim, T. Reindl, R. Riither, Comparative Analysis of Albedo Measurements (Plane-of-array Horizontal Satellite) at Multiple Sites Worldwide, 2019.